8-21-2014

# Nonanalytic behavior of the Casimir force across a Lifshitz transition in a spin-orbit-coupled material

Andrew A. Allocca
*University of Maryland, College Park*

Justin H. Wilson
*University of Maryland, College Park*

Victor Galitski
*University of Maryland, College Park*



## Recommended Citation

Allocca, A., Wilson, J., & Galitski, V. (2014). Nonanalytic behavior of the Casimir force across a Lifshitz transition in a spin-orbit-coupled material. *Physical Review B - Condensed Matter and Materials Physics, 90* (7) https://doi.org/10.1103/PhysRevB.90.075420

# Nonanalytic behavior of the Casimir force across a Lifshitz transition in a spin-orbit-coupled material

Andrew A. Allocca, Justin H. Wilson, and Victor Galitski

Phys. Rev. B **90**, 075420 — Published 21 August 2014

DOI: 10.1103/PhysRevB.90.075420

# Non-analytic behavior of the Casimir force across a Lifshitz transition in a spin-orbit coupled material

Andrew A. Allocca, Justin H. Wilson, and Victor Galitski
*Joint Quantum Institute and Condensed Matter Theory Center, Department of Physics, University of Maryland, College Park, Maryland 20742-4111, USA*

The Casimir effect is a fascinating phenomenon where quantum fluctuations of the electromagnetic field give rise to measurable forces between macroscopic systems. Here we propose that Casimir effect can be used as a tool to detect changes in electronic structures. In particular, we focus here on the Lifshitz transition - a topological change in the Fermi surface - in a planar spin-orbit coupled semiconductor in a magnetic field and calculate the Casimir force between the semiconductor and another probe system across the magnetic-field-tuned transition. We show that the Casimir force experiences a sharp kink at the topological transition and provide numerical estimates indicating that the effect is well within experimental reach. The simplest experimental realization of the proposed effect would involve a metal-coated sphere suspended from a micro-cantilever above a thin layer of InSb (or another semiconductor with a large $g$-factor).

## I. INTRODUCTION

In 1948, Casimir predicted attraction between two neutral, perfectly conducting materials[1], and after nearly fifty years of theory[2], experimental evidence was presented by Lamoreaux[3]. Following this discovery there was a flurry of theory[4] and experiment[5] which led to an astounding amount of theoretical and experimental machinery. With this machinery, others have observed that the Casimir force can have a non-trivial dependence on material parameters[6–9], some of which may be tunable. We continue in this direction, considering how the Casimir force changes as a parameter tunes a system across a Lifshitz transition – an extreme case of Fermi surface reconstruction in an electronic material. Unusual for the Casimir effect, we find that as the system goes through this transition by tuning a magnetic field, the Casimir force is both non-analytic and non-monotonic as a function of the field. Our model involves a thin layer of indium antimonide (or another semiconductor with a large $g$-factor, as discussed below) and could be experimentally realized in the common experimental setup for Casimir measurements as shown in Fig. 1.

The Casimir effect for real materials, as first developed by Lifshitz[10], explicitly depends on the electromagnetic response of a material. This response can be built into the boundary conditions of the electromagnetic field itself. Diagrammatically, the Casimir energy between two plates $A$ and $B$ takes the schematic form

$\mathcal{E}_c =$ 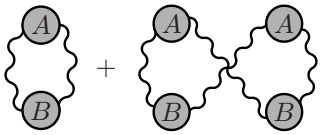 (1)


where 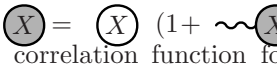 is the dressed current-current correlation function for plate $X$ while  is the usual current-current correlator derived in linear response theory – a material dependent quantity related to conductivity. It enters the expression in a crucial way, and thus, features in the frequency-dependent conductivity translate to features in the Casimir force. Being able to tune the Casimir force by modifying this frequency-dependent conductivity[11] could have important applications for precision gravity experiments[12] and applications to nanotechnology[13].

From the other direction, and importantly for the subject of this paper, any change of the Casimir force would be an indication of a change in the material's properties. Special geometries[14] and boundary conditions[15] can change the Casimir force to be repulsive, though with symmetric geometries without time-reversal symmetry breaking, one cannot escape an attractive effect[16]. Just as a repulsive effect would be a signature of some time-reversal symmetry breaking (such as in the case of two quantum Hall plates[17] or topological insulators with gapped surface states[18]), other changes in the Casimir force can be attributed to other material properties. For instance, Bimonte and coauthors showed that one can in principle measure the change in Casimir energy between a normal and superconducting state[7]. Additionally, it has been demonstrated that both the Casimir effect and the thermal Casimir effect[8] are capable of probing phase transitions[9].

In this paper, we consider how the Casimir force

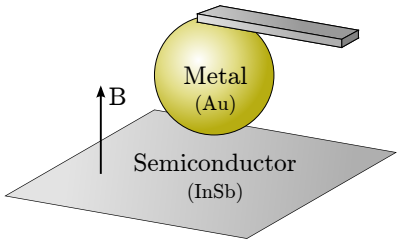


FIG. 1. The geometry typically used in experimental measurements of the Casimir force is a gold coated sphere suspended above a planar plate from a cantilever. We consider a lower plate of indium antimonide with an applied magnetic field.

changes as we tune a two-dimensional spin-orbit coupled material through a Lifshitz transition. A Lifshitz transition occurs when a material's Fermi surface undergoes a topological change – such as the emergence or collapse of an electron or hole pocket[19]. Various models are suspected to undergo some type of Lifshitz transition[20] including the cuprates[21], and experimental evidence of a Lifshitz transition has been recently observed in iron arsenic superconductors[22]. We will first define our model and show how it undergoes such a transition. Introducing the expression for the Casimir energy, we then find the current-current correlator in linear response theory after minimally coupling our Hamiltonian to a vector potential. Using this expression, we numerically integrate to obtain the Casimir force as we tune our original Hamiltonian through a Lifshitz transition. We end with some discussion of this feature.

## II. THEORETICAL MODEL

Others have considered the consequences on the Casimir effect of considering two-dimensional plates instead of thick slabs[23,24], but similar to the particular case of graphene[25], our model requires a more microscopic approach (see Appendix A). We consider the Casimir force at zero temperature between two parallel plates where at least one is modeled as a two-band spin-orbit coupled material (sufficiently thin to be considered quasi-two dimensional) with a fixed chemical potential and tunable Zeeman splitting due to an external magnetic field. (When considering only one spin-orbit coupled plate, the other is a metallic plate, modeled as a clean free electron gas.) The Zeeman field tunes a gap in this two-band material and causes one of the Fermi surfaces to form or collapse. This is the simplest realistic model exhibiting a Lifshitz transition. At these transition points, the Casimir force between the two plates experiences a kink, as seen in Fig. 2.

This could be experimentally measured with the usual plate and sphere geometry as seen in Fig. 1. The plate would be a thin layer of InSb while the sphere would be the usual Au-coated sphere. While we consider the parallel plate scenario, our calculations can be generalized to the sphere-plate geometry by using the proximity force approximation[4] without damage to the non-analyticity we observe in the Casimir force.

We consider the single-particle effective Hamiltonian for the conduction bands of the semiconductor,

$$\hat{H} = \frac{k^2}{2m^*} - \mu + \beta(\hat{\sigma}_x k_x - \hat{\sigma}_y k_y) + V_z \hat{\sigma}_z, \qquad (2)$$

which has eigenvalues

$$\xi^{\pm}(k) = \frac{k^2}{2m^*} - \mu \pm \sqrt{V_z^2 + \beta^2 k^2}, \qquad (3)$$

where $m^*$ and $\mu$ are the conduction band effective mass of the electron and chemical potential. The coefficient

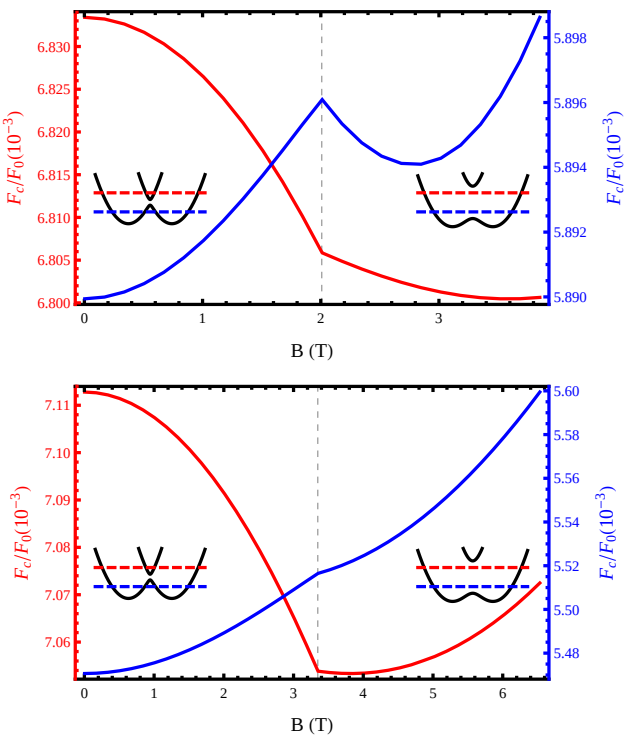


FIG. 2. (Color online) The Casimir force $F_c$ normalized by the ideal conductor value between one semiconductor plate and one metallic plate separated by $a = 50\,\text{nm}$ as a function of applied magnetic field. The red plot (left axis) corresponds to $\mu > 0$, and the blue plot (right axis) corresponds to $\mu < 0$. The upper plot uses $\mu = \pm 6\,\text{meV}$ and the lower uses $\mu = \pm 10\,\text{meV}$. The insets show the band structure above and below the transition point (marked with a dashed line) along with the two fixed values of the Fermi energy.

$\beta$ is the strength of the Dresselhaus spin-orbit coupling, and $\sigma_i$ are the Pauli matrices. The factor $V_z$ is the induced Zeeman splitting, given by $V_z = \mu_B g^* B$, where $\mu_B$ is the Bohr magneton, $g^*$ is the material's $g$-factor, and $B$ is an applied magnetic field. For all calculations we will assume that this Hamiltonian is a simple model of the the relevant bands of the material indium antimonide, for which $m^* = 0.014 m_0$ , where $m_0$ is the free electron mass, and $\beta = \gamma\langle k_z^2\rangle \simeq \gamma\left(\frac{\pi}{d}\right)^2$[26], where $d$ is the thickness of the plate and $\gamma = 760.1\,\text{eV\AA}^3$ is the intrinsic Dresselhaus parameter for the material. We consider InSb plates that are six lattice constants thick, $d = 6 \times 0.6479\,\text{nm} = 3.89\,\text{nm}$. The plates may still be considered effectively 2D as long as the energy needed to excite higher electron modes in the confined direction is much larger than the energy requires to excite the two lowest bands modeled here. Additionally, since the $g$-factor of InSb is $g^* = -51.6$ we can also neglect the orbital coupling of the electrons directly to the external magnetic field as well as the effect of the magnetic field on the metallic plate when it is considered[27].

This model is a simplification since we neglect virtual

excitations in the confined direction as well as changes in bulk parameters due to confining, band bending, and emergence of other spin-orbit effects (e.g. Rashba spin-orbit coupling). The parameters are at least of the same order of magnitude, and other spin orbit terms just modify the geometry of the Fermi surface. At worst, these complications and effects due to the crystalline structure of InSb, should affect the quantitative but not qualitative features we find.

For $\mu > |V_z|$ there are two bands crossing the Fermi energy. With fixed $\mu$, as $|V_z|$ is increased the occupation of the upper band decreases until the Fermi surface disappears entirely when $|\mu| = |V_z|$ – the electron pocket defined by that Fermi surface disappears. Increasing the Zeeman splitting further, the Fermi energy lies within the gap and only the lower band crosses the Fermi level, giving a single Fermi surface. This represents the Lifshitz transition for $\mu > 0$, and is shown with the red dashed line in the insets of Fig. 2.

If $m^*\beta^2 > |V_z|$ the lower band has a local maximum at $k = 0$ and a similar scenario can be considered for $\epsilon_{\min} < \mu < -|V_z|$, where $\epsilon_{\min}$ is the lowest energy of the lower band. In this case, the lower band crosses the Fermi energy for two distinct values of $k$, producing two Fermi surfaces – the inner one enclosing a hole pocket. Again, increasing $|V_z|$ for fixed $\mu$ leads to a shrinking of the inner Fermi surface until it disappears completely at the point when $|\mu| = |V_z|$. For larger Zeeman splitting, the Fermi energy again lies within the gap and there is a single Fermi surface. This senario for $\mu < 0$ is shown with the blue dashed line in the insets of Fig. 2. The disappearance of a Fermi surface by changing $V_z$ in these two scenarios are simple examples of a Zeeman-driven Lifshitz transition.

Since these transitions occur at a specific value of $|V_z|$, regardless of the sign of $V_z$, the direction of the applied magnetic field is unimportant. For this reason, we will always assume $V_z > 0$ for simplicity. We will also denote the magnetic field strength needed to reach the Lifshitz transition point as $B_L = \frac{|\mu|}{g\mu_B}$.

We use a microscopic quantum field theoretic method to calculate the Casimir energy at zero temperature in terms of the current-current correlation functions of the two electron systems under consideration and virtual photons in the 3D vacuum between them. Summing up the diagrams in Eq. (1), the Casimir energy at zero temperature for parallel 2D plates separated by a distance $a$ is given by

$$\mathcal{E}_c(a) = \frac{1}{4\pi^2}\int_0^\infty dq_\perp\, q_\perp \int_0^{q_\perp} d\omega\ \mathrm{tr}\ln\left[\hat{\mathbf{1}} - \hat{\tilde{\Pi}}_A(q_\perp, i\omega)\hat{D}(q_\perp, i\omega, a)\hat{\tilde{\Pi}}_B(q_\perp, i\omega)\hat{D}(q_\perp, i\omega, a)\right], \tag{4}$$

where $\hat{D}$ is the photon propagator and $\hat{\tilde{\Pi}}_i$ is the current-current correlation function for plate $i$, dressed by interactions with 3D photons. We choose the gauge with no scalar potential, $\phi = 0$, so the relevant components of the photon propagator have the form

$$\hat{D}(q_\perp, i\omega, z) = \frac{\hbar}{2}\begin{pmatrix} \frac{q_\perp}{\omega^2} & 0 \\ 0 & \frac{1}{q_\perp}\end{pmatrix} e^{-q_\perp|z|}.$$

The dressed current-current correlation function can be expressed in terms of the bare correlation function, $\hat{\Pi}$, as

$$\hat{\tilde{\Pi}} = \left[\hat{\mathbf{1}} - \hat{\Pi}\hat{D}(z=0)\right]^{-1}\hat{\Pi},$$

which accounts for dynamical screening of photons in the random phase approximation (RPA). A more thorough derivation of Eq. (4) is given in Appendix A for completeness.

We determine the bare correlation function using the current operator, $j_i(x) = \psi^\dagger(x)\frac{\partial \hat{H}[A]}{\partial A_i(x)}\psi(x)$, where $\hat{H}[A]$ is the Hamiltonian given in Eq. (2) after minimal coupling. The correlation function is then expressed in terms of the current as,

$$\Pi_{ij}(x, x') = \langle -\delta(x-x')\delta_{ij}\partial_{A_i} j_i(x) + j_i(x)j_j(x')\rangle\Big|_{A=0}, \tag{5}$$

where $\langle\cdots\rangle$ represents averaging over the ground state[28]. In the case of a weakly correlated system we can use the approximation that the Casimir effect is determined by the local current-current response functions, i.e. we only need to consider the $q = 0$ limit of $\hat{\Pi}$ since non-local behavior is screened out. Equivalently, this is a simple extension of the usual plasma model to a spin-orbit coupled Hamiltonian, which describes the plates. Furthermore, coupling of the spin to the magnetic fluctuations of the vacuum field do not need to be considered. In this limit, the correlation function for the spin-orbit coupled plates has the form

$$\hat{\Pi}(i\omega) = -\frac{e^2}{h}\begin{pmatrix} \Pi_L(i\omega) & \Pi_H(i\omega) \\ -\Pi_H(i\omega) & \Pi_L(i\omega)\end{pmatrix}, \tag{6}$$

where $e^2/h$ is the quantum of conductance,

$$\Pi_H(i\omega) = V_z\left[\cot^{-1}\left(\frac{\omega}{2\epsilon^+}\right) - \cot^{-1}\left(\frac{\omega}{2\epsilon^-}\right)\right] \tag{7}$$

$$\Pi_L(i\omega) = \mu\left[\Theta(\mu - |V_z|) + \Theta(\mu + |V_z|)\right] + \frac{\epsilon^+ - \epsilon^-}{2} + \frac{\omega^2 - 4V_z^2}{4V_z\omega}\Pi_H(i\omega) \tag{8}$$

and $\epsilon^{\pm}$ are the positive square roots of

$$(\epsilon^{\pm})^2 = V_z^2 + \max\left\{0, 2m^*\beta^2(\mu + m^*\beta^2)\left[1 \pm \sqrt{1 - \frac{\mu^2 - V_z^2}{(\mu + m^*\beta^2)^2}}\right]\right\}. \quad (9)$$

## III. RESULTS

We take the derivative of Eq. (4) with respect to the plate separation, $a$, to obtain an expression for the Casimir force. We then integrate this expression numerically for fixed separation $a = 50\,\text{nm}$ and Fermi energy $\mu$, while varying $|V_z|$ – i.e., varying the magnetic field in an actual experiment. We consider two Fermi energies, $\mu = \pm 6\,\text{meV}$ and $\pm\,10\,\text{meV}$, which give that the magnetic fields needed to reach the transition are $B_L = 2\,\text{T}$ and $3.35\,\text{T}$. For all numerical results, we will give the Casimir force in our considered system, $F_c$, normalized by the Casimir force between ideal conducting plates, $F_0 = -\hbar c\pi^2/240a^4$, calculated for the same plate separation. The dependence on plate separation closely follows the usual dependence for the Casimir force with the magnitude of the force increasing at shorter separations. Furthermore, the qualitiative nature of the effect we find is not affected by the plate separation.

For the simple system with *no* spin-orbit coupling ($\beta = 0$), i.e. two metallic plates, the Casimir force as a function of magnetic field is shown in Fig. 3. As the magnetic field is tuned and the chemical potential is kept fixed, the Fermi surface changes by the removal of an electron pocket

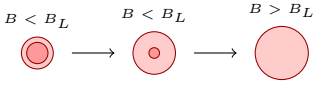


, $\mu > 0$ fixed, (10)

where the shaded circles represent filled electron states in the 2D $k$-space. In Fig. 3, we see that for $B < B_L$ the Casimir force is constant with varying $B$, since the carrier density of the material, which in this case is the only free parameter determining the value of $\hat{\Pi} = -\frac{e^2}{h}\left[2\mu\,\Theta(\mu - |V_z|) + (\mu + |V_z|)\,\Theta(|V_z| - \mu)\right]$, is constant in this region. As the upper band is raised above the Fermi level, the closing of the upper band Fermi surface is indicated by a kink in the Casimir force, above which the magnitude of the force increases with $B$, consistent with the increase in the carrier density in this region. Unlike spin-orbit coupled materials – the subject of this paper – this simple system has a critical field $B_L = \frac{|\mu|}{g\mu_B}$ which is unreasonably large (on the order of 10000 T) due to large Fermi energies and small $g$-factors. However, the spin-orbit coupled semiconductors have small Fermi energies and large $g$-factors, leading to a more reasonable value of $B_L$.

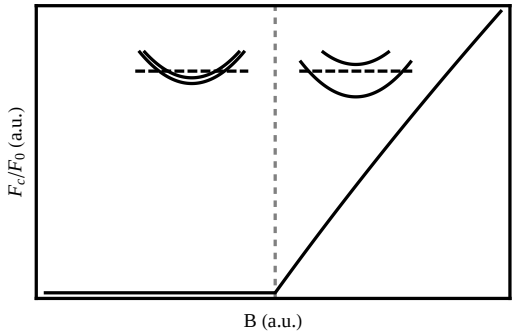


FIG. 3. The Casimir force $F_c$ normalized by the ideal conductor value between two metallic plates at a fixed separation as a function of the applied magnetic field. The insets show the band structure above and below the transition along with the fixed value of the Fermi energy. With a large Fermi energy and small electronic $g$-factor ($\approx 2$), a prohibitively large magnetic field is needed to reach the transition.

| $\mu$ (meV) | $\frac{F_c(B_L)}{F_0}$ | $\frac{F_c(B_L)-F_c(0)}{F_0}$ | $\frac{dF_c}{dB}\|_{B=B_L^+} - \frac{dF_c}{dB}\|_{B=B_L^-}$ ($F_0$/T) |
|---|---|---|---|
| 6 | 6.806 | -0.02756 | 0.0212 |
| 10 | 7.054 | -0.0589 | 0.0326 |
| -6 | 5.896 | 0.0061 | -0.0097 |
| -10 | 5.516 | 0.0458 | -0.0125 |

TABLE I. Some important numerical results from the case of the Casimir force between one metallic plate and one InSb plate, all in units of $F_0 = -\hbar c\pi^2/240a^4 \times 10^{-3}$. The first column gives the value of the force at the transition. The second column gives the change in the force from $B = 0$ to the transition. The last column gives the jump in the derivative of the force with respect to applied magnetic field across the transition, giving a measure of the severity of the kink.

For the semi-conductors under consideration, the Casimir force as a function of magnetic field is presented in Fig. 2 for the case of one metallic plate and one InSb plate, and in Fig. 4 for the case of two InSb plates. Additionally, relevant numerical quantities (chemical potential, value of the force, change of force from the zero magnetic field value, and the change of the slope characterizing the kink) associated with these plots are given in Table I and Table II. As the Zeeman energy changes, the value of the chemical potential has a strong influence on the behavior of the Casimir force. For positive values of $\mu$ (red curves), the Fermi surface sees behavior similar to that seen in Eq. (10). The behavior of the Casimir force above and below the transition is similar in both systems we consider, with the force decreasing in magnitude as the magnetic field strength is increased towards the transition, and the force increasing above the transition for large enough values of $B$. This increase at large $B$ is irrespective of Fermi energy or case, and $V_z \gg \beta\sqrt{2m^*|\mu|}$, leading to a suppresion of the spin-orbit coupling term and a cross-over to the simple metallic behavior.

For negative values of $\mu$ (blue curves), the InSb Fermi

| $\mu$ (meV) | $\frac{F_c(B_L)}{F_0}$ | $\frac{F_c(B_L)-F_c(0)}{F_0}$ | $\frac{dF_c}{dB}\|_{B=B_L^+} - \frac{dF_c}{dB}\|_{B=B_L^-}$ ($F_0$/T) |
|---|---|---|---|
| 6 | 5.138 | -0.0291 | 0.0200 |
| 10 | 5.346 | -0.0619 | 0.0310 |
| -6 | 4.367 | -0.0020 | -0.0056 |
| -10 | 4.041 | 0.0192 | -0.0035 |

TABLE II. The same as Table I but for the case of two identical InSb plates.

surface changes begins with a hole pocket that disappears at the critical magnetic field

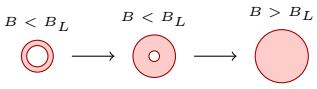


$$\mu < 0 \text{ fixed}, \qquad (11)$$

where now the empty hole is the hole pocket. the behavior of the Casimir force is different in the two systems. When considering one InSb plate and one metallic plate, the force increases with increasing $B$ below the Lifshitz transition for all values of $\mu$ considered, and then increases above the transition as well for a strong enough magnetic field (again, in a cross-over to the simple metal case). In the system composed of two InSb plates, there is no common trend seen in the Casimir force for the negative values of the Fermi energy we consider, except that, again, above a certain magnetic field strength the force increases with increasing $B$. For the lowest of the Fermi energies considered, we see that the Casimir force decreases with $B$ below the transition, then even more quickly directly above the transition.

The main feature of all of these plots is the sharp kink seen at the Lifshitz transition point, and this feature should be discernable even considering the effects of temperature and a substrate. We expect the features to reimain for temperatures much less than the energy of the gap at the transition point (i.e. the chemical potential): 70 K and 116 K for chemical potentials of 6 meV and 10 meV respectively. Additionally, as long as the substrate for either the InSb or Au is a poor conductor, non-magnetic, and does not experience an electronic transition in the range of magnetic fields needed to reach the Lifshitz transition then we would expect it to have at most a small effect on our results, and not to change the nature of features we find.

## IV. CONCLUSIONS

These features can be understood by examining the imaginary frequency AC conductivities of the InSb plates as a function of magnetic field at a fixed non-zero frequency; since the plates have no disorder there is no dissipation and the longitudinal DC conductivity is infinite. Both the longitudinal and Hall conductivities at finite frequency have a discontinuity in their derivatives with respect to $B$ at the point where $|\mu| = V_z$, just as we find with the Casimir force. The overall trend in the

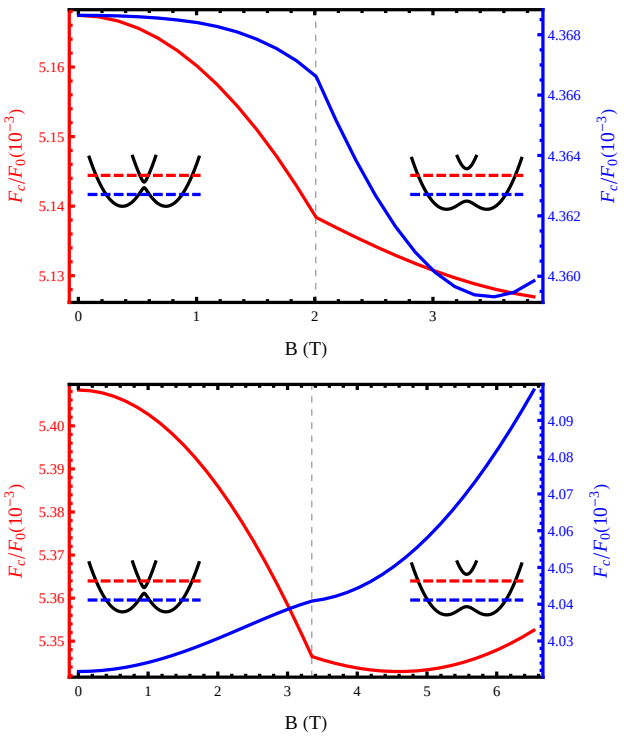


FIG. 4. (Color online) The Casimir force $F_c$ normalized by the ideal conductor value $F_0$ between two semiconductor plates separated by $a = 50$ nm as a function of applied magnetic field. The red plot (left axis) corresponds to $\mu > 0$, and the blue plot (right axis) corresponds to $\mu < 0$. The upper plot uses $\mu = \pm 6$ meV and the lower uses $\mu = \pm 10$ meV. The insets show the band structure above and below the transition point along with the two fixed values of the Fermi energy.

longitudinal conductivity, shown in Fig. 5 mimicks the behavior of the Casimir force we find for positive Fermi energies—decreasing in magnitude below the transition, then decreasing less drastically directly above the transition until reaching a minimum and increasing with $B$. All of these results taken together suggest that the Hall contribution to the Casimir effect from interband spin-orbit interactions, which are stronger when the bands are closer in energy (i.e. small $V_z$), works to suppress the strength of the Casimir force. Since the Lifshitz transition occurs precisely when $V_z = |\mu|$, for smaller values of the Fermi energy the transition occurs for smaller values of $V_z$, meaning that the bands are not so far removed from each other and interband effects are stronger. Additionally, these effects are stronger in the system with two InSb plates, as would be expected if they are the result of spin-orbit coupling.

As we have shown, tuning through a Lifshitz transition in this material causes a kink in the Casimir force while the microscopics control the nature and severity of the kink. We expect similar features to be found in other materials with such transitions – particularly due to the change in the carrier concentration across such a

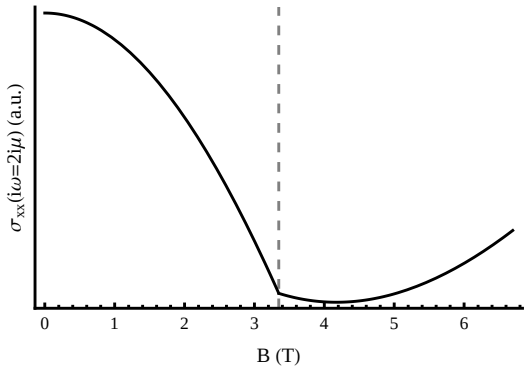


FIG. 5. The imaginary frequency longitudinal conductivity of the InSb plate at $i\omega = 2i\mu$ for $\mu = 10\,\text{meV}$ as a function of applied magnetic field. The Lifshitz transition point is indicated with a dashed line.

transition. This is one way in which precision Casimir force experiments could be used as a probe of nontrivial electronic properties or transitions. This is not exclusive to the particular semiconductor considered here; not only could the Casimir effect be used to probe Lifshitz transitions in other materials, but it could conceivably be used to detect other phenomena such as the Fermi surface reconstruction and the superconducting transition in cuprates and disorder-driven phenomena such as localization.

## V. ACKNOWLEDGEMENTS

This work was supported by DOE-BES DESC0001911 (A.A. and V.G.), JQI-PFC (J.W.), and the Simons Foundation. We would like to thank Doron Bergmann, Jeremy Munday, and Jing Xia for useful discussions.

### Appendix A: Derivation of the Casimir Energy

We wish to derive an expression for the electromagnetic Casimir energy between two parallel two-dimensional plates in terms of photon propagators and quantities that can be derived from the microscopic description of the electrons in each plate. We do this by calculating the free energy of the two plate system interacting with three-dimensional photons, then subtracting off the contribution for each isolated plate and the photon background, leaving only the part coming from interactions between the plates,

$$\begin{aligned}\mathcal{E}_c &= F - F_1 - F_2 \\ &= -\frac{1}{\beta}\left(\ln \mathcal{Z} - \ln \mathcal{Z}_1 - \ln \mathcal{Z}_2\right) \\ &= -\frac{1}{\beta}\left(\ln \int \mathcal{D}A\, e^{-S_{EM}-S_1-S_2} \right. \\ &\qquad \left. - \sum_{i=1}^{2} \ln \int \mathcal{D}A_i\, e^{-S_{EM}-S_i}\right).\end{aligned}$$

Here, $F$ and $\mathcal{Z}$ are the free energy and partition function of the full system composed of two plates interacting with three-dimensional photons, while $F_i$ and $\mathcal{Z}_i$ are the free energy and partition function of plate $i$ interacting with three-dimensional photons in isolation. The partition functions are calculated as path integrals over the photon field $A$, with the actions for the photon field given by

$$S_{EM}[A] = -\frac{1}{4}\int d^4x\, F_{\mu\nu}F^{\mu\nu},$$

where $F_{\mu\nu}$ is the electromagnetic field tensor, and the action for the electrons in plate $i$ given by

$$S_i[A] = -\frac{1}{2}\sum_n \int \frac{d^2q}{(2\pi)^2} A^\mu(q, z_i)\,\Pi_{\mu\nu,i}(q)\,A^\nu(-q, z_i).$$

Throughout we have also set $\hbar = c = 1$, and we use the shorthand $\pm q = (\pm\vec{q}, \omega_n)$. The two plates are located at $z = z_1$ and $z = z_2$ with $z_2 - z_1 = a$, the distance between the plates. This expression for $S_i$ is obtained from linear response theory, with $\Pi$ given by Eq. (5). In principle, higher order terms with internal photon lines and two external photon lines could be included as well, but they would be higher order in $\alpha = \frac{e^2}{4\pi} \approx \frac{1}{137}$ and therefore provide only small corrections.

Introducing the notation

$$\int \mathcal{D}A\,(\cdots)e^{-S_{EM}[A]} = \langle\cdots\rangle_A,$$

noting that the lns serve to keep only connected diagrams, and that we have subtracted off diagrams that involve only single plates, we now have that the Casimir energy can be written as,

$$\begin{aligned}\mathcal{E}_c &= -\frac{1}{\beta}\left(\ln\left\langle e^{-S_1[A]-S_2[A]}\right\rangle_A - \ln\left\langle e^{-S_1[A_1]-S_2[A_2]}\right\rangle_{A_{1,2}}\right) \\ &= -\frac{1}{\beta}\left\langle e^{-S_1[A]-S_2[A]}\right\rangle_{A,\text{ connected, both plates}} \qquad \text{(A1)}\end{aligned}$$

We are left with two types of connected diagrams, shown in Fig. 6

The second type of diagram demonstrated in Fig. 6 dresses the interaction of the photons with the plates. Carefully keeping track of the coefficients in the expansion of Eq. (A1) calculating the symmetry factors of such

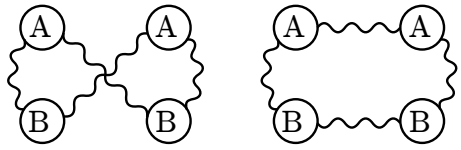


FIG. 6. Examples of the two types of diagrams we are left with. In the first type, all photon lines connect one plate (in the form of $\hat{\Pi}_1$, labelled here by A) to the other plate (in the form of $\hat{\Pi}_2$, labelled by B). In the second type, there is at least a single photon line connecting a plate to itself.

diagrams, we find that we may define the photon-dressed current-current correlation function as

$$\hat{\tilde{\Pi}} = \hat{\Pi} + \hat{\Pi}\hat{D}(z=0)\hat{\Pi} + \cdots = \left[\hat{\mathbf{1}} - \hat{\Pi}\hat{D}(0)\right]^{-1}\hat{\Pi} \quad \text{(A2)}$$

and we are left with only the first type of diagrams, but with $\hat{\Pi}$ replaced with $\hat{\tilde{\Pi}}$. This is equivalent to considering the random phase approximation (RPA) for the total current-current correlation. Using this definition and calculating the appropriate coefficient for each diagram, we can write a single expression that incorporates all connected diagrams. Suppressing all frequency and momentum labels, we can write

$$\begin{aligned}\mathcal{E}_c(a) &= -\frac{1}{\beta}\sum_n \int \frac{d^2q}{(2\pi)^2}\,\mathrm{tr}\left[\sum_{k=1}^{\infty}\frac{1}{2k}\left(\hat{\tilde{\Pi}}_1\hat{D}(a)\hat{\tilde{\Pi}}_2\hat{D}(a)\right)^k\right] \\ &= \frac{1}{2\beta}\sum_n \int \frac{d^2q}{(2\pi)^2}\,\mathrm{tr}\ln\left[\hat{\mathbf{1}} - \hat{\tilde{\Pi}}_1\hat{D}(a)\hat{\tilde{\Pi}}_2\hat{D}(a)\right] \\ &\overset{T\to 0}{=} \frac{1}{2}\int_{-\infty}^{\infty}\frac{d\omega}{2\pi}\int\frac{d^2q}{(2\pi)^2}\,\mathrm{tr}\ln\left[\hat{\mathbf{1}} - \hat{\tilde{\Pi}}_1\hat{D}(a)\hat{\tilde{\Pi}}_2\hat{D}(a)\right]\end{aligned}$$

In the limit $T \to 0$, we have not performed the analytic continuation $i\omega_n \to \omega + i0^+$, we simply make the discrete Matsubara sum into a continuous integral over imaginary frequency. Assuming that the integrand depends only on the magnitude of $\vec{q}$ and not its direction, we may perform the angular integration. We now perform a convenient change of variables, defining $q_\perp = \sqrt{\omega^2 + q^2}$. This is simply a formal change of variables that makes the expression simpler to integrate numerically. With this change of variables and a reordering of integrals we arrive at the final expression for the Casimir energy given in Eq. (4).


[1] H. B. G. Casimir, Proc. K. Ned. Akad. Wet. **51**, 793 (1948).
[2] K. A. Milton, *The Casimir Effect*, Physical Manifestations of Zero-point energy (World Scientific, 2001).
[3] S. K. Lamoreaux, Phys. Rev. Lett. **78**, 5 (1997).
[4] M. Bordag, U. Mohideen, and V. M. Mostepanenko, Phys. Rep. **353**, 1 (2001); K. A. Milton, J. Phys.: Conference Series **161**, 012001 (2009), 0806.2880.
[5] M. Sparnaay, Nature **180**, 334 (1957); Physica **24**, 751 (1958); S. K. Lamoreaux, Rep. Prog. Phys. **68**, 201 (2005); U. Mohideen and A. Roy, Phys. Rev. Lett. **81**, 4549 (1998); J. N. Munday, F. Capasso, and V. A. Parsegian, Nature (London) **457**, 170 (2009); A. A. Banishev, G. L. Klimchitskaya, V. M. Mostepanenko, and U. Mohideen, Phys. Rev. Lett. **110**, 137401 (2013), 1211.1470v2.
[6] P. Bruno, Phys. Rev. Lett. **88**, 240401 (2002); G. Metalidis and P. Bruno, Phys. Rev. A **66**, 062102 (2002).
[7] G. Bimonte, E. Calloni, G. Esposito, L. Milano, and L. Rosa, Phys. Rev. Lett. **94**, 180402 (2005); G. Bimonte, G. Bimonte, E. Calloni, E. Calloni, G. Esposito, G. Esposito, L. Rosa, and L. Rosa, Nucl. Phys. B **726**, 441 (2005).
[8] A. O. Sushkov, W. J. Kim, D. Dalvit, and S. K. Lamoreaux, Nature Phys. **7**, 230 (2011).
[9] G. Torricelli, P. J. van Zwol, O. Shpak, C. Binns, G. Palasantzas, B. J. Kooi, V. B. Svetovoy, and M. Wuttig, Phys. Rev. A **82**, 010101 (2010); P. Ziherl, R. Podgornik, and S. Žumer, Chem. Phys. Lett. **295**, 99 (1998).
[10] E. M. Lifshitz, Sov. Phys. JETP **2**, 73 (1956); I. E. Dzyaloshinskii, E. M. Lifshitz, and L. P. Pitaevskii, Sov. Phys. Usp. **4**, 153 (1961).
[11] F. Chen, G. L. Klimchitskaya, V. M. Mostepanenko, and U. Mohideen, Phys. Rev. B **76**, 035338 (2007); S. de Man, K. Heeck, R. J. Wijngaarden, and D. Iannuzzi, Phys. Rev. Lett. **103**, 040402 (2009); C.-C. Chang, A. A. Banishev, G. L. Klimchitskaya, V. M. Mostepanenko, and U. Mohideen, Phys. Rev. Lett. **107**, 090403 (2011).
[12] M. Bordag, B. Geyer, G. L. Klimchitskaya, and V. M. Mostepanenko, Phys. Rev. D **58**, 075003 (1998); J. C. Long, H. W. Chan, A. B. Churnside, E. A. Gulbis, M. C. M. Varney, and J. C. Price, Nature **421**, 922 (2003); R. S. Decca, D. López, H. B. Chan, E. Fischbach, D. E. Krause, and C. R. Jamell, Phys. Rev. Lett. **94**, 240401 (2005); D. J. Kapner, T. S. Cook, E. G. Adelberger, J. H. Gundlach, B. R. Heckel, C. D. Hoyle, and H. E. Swanson, **98**, 021101 (2007); D. M. Weld, J. Xia, B. Cabrera, and A. Kapitulnik, Phys. Rev. D **77**, 062006 (2008).
[13] F. Capasso, J. N. Munday, D. Iannuzzi, and H. B. Chan, IEEE J. Sel. Topics Quantum Electron. **13**, 400 (2007).
[14] M. Levin, A. P. McCauley, A. W. Rodriguez, M. T. H. Reid, and S. G. Johnson, Phys. Rev. Lett. **105**, 090403 (2010), 1003.3487.
[15] S. A. Fulling, L. Kaplan, and J. H. Wilson, Phys. Rev. A **76**, 012118 (2007).
[16] O. Kenneth and I. Klich, Phys. Rev. Lett. **97**, 160401 (2006).
[17] W.-K. Tse and A. H. MacDonald, Phys. Rev. Lett. **109**, 236806 (2012).
[18] A. G. Grushin and A. Cortijo, Phys. Rev. Lett. **106**, 020403 (2011).
[19] I. M. Lifshitz, Sov. Phys. JETP **38**, 1569 (1960); A. A. Abrikosov, *Fundamentals of the theory of metals* (North-Holland, Amsterdam, 1988).
[20] K. S. Chen, Z. Y. Meng, T. Pruschke, J. Moreno, and

M. Jarrell, Phys. Rev. B **86**, 165136 (2012); Y. Okamoto, A. Nishio, and Z. Hiroi, **81**, 121102 (2010); A. Hackl and M. Vojta, Phys. Rev. Lett. **106**, 137002 (2011).

[21] M. R. Norman, J. Lin, and A. J. Millis, Phys. Rev. B **81**, 180513 (2010).

[22] C. Liu, T. Kondo, R. M. Fernandes, A. D. Palczewski, E. D. Mun, N. Ni, A. N. Thaler, A. Bostwick, E. Rotenberg, J. Schmalian, S. L. Bud'ko, P. C. Canfield, and A. Kaminski, Nature Phys. **6**, 419 (2010).

[23] P. Parashar, K. A. Milton, K. V. Shajesh, and M. Schaden, Phys. Rev. D **86**, 085021 (2012).

[24] G. Barton, Journal of Physics A: Mathematical and General **38**, 2997 (2005); **38**, 3021 (2005).

[25] M. Bordag, I. V. Fialkovsky, D. M. Gitman, and D. V. Vassilevich, Phys. Rev. B **80**, 245406 (2009); D. Drosdoff and L. M. Woods, Phys. Rev. B **82**, 155459 (2010); B. E. Sernelius, EPL (Europhysics Letters) **95**, 57003 (2011).

[26] J. D. Koralek, C. P. Weber, J. Orenstein, B. A. Bernevig, S.-C. Zhang, S. Mack, and D. D. Awschalom, Nature **458**, 610 (2009).

[27] R. Winkler, *Spin–Orbit Coupling Effects in Two-Dimensional Electron and Hole Systems*, Springer Tracts in Modern Physics, Vol. 191 (Springer Berlin Heidelberg, Berlin, Heidelberg, 2003).

[28] A. Altland and B. D. Simons, *Condensed Matter Field Theory*, 2nd ed. (Cambridge University Press, Cambridge, 2010).